Analysis of Nonlinear Termination Networks for Coupled Lossy and Dispersive Transmission Lines

George W. Pan, Gaofeng Wang, and Barry K. Gilbert

Abstract— **Based upon an algorithm described in a separate paper [1], multiple transmission lines with skin effect losses and dispersive characteristics were analyzed by the volume equivalent principle, and the scattering matrix $[S\omega]$ and characteristic impedance matrix $[Z_0\omega]$ of the transmission lines were obtained. The $[S\omega]$ and $[Z_0(w)]$ were then transformed by the inverse FFT into the time domain. The scattering matrix representation is multiplicative in nature, which leads to the time domain formulation as a set of convolution integrals.**

Instead of attempting to solve a set of coupled convolution integral equations by the multivariable Newton–Raphson method, which may occasionally be unstable, we generated a set of object functions and applied a multivariable optimization technique, referred to as the modified Levenberg-Marquardt algorithm, to attain the solutions. The new method, which is quite general, reduces to the special cases derived in many previous publications.

I. Introduction

Coupled lossy and dispersive transmission lines connected to active devices are commonly found in the packaging of high-speed, high density digital electronics. These devices, including diodes, transistors, voltage limiters and so forth, acting as sources or terminations, have their output or input impedances as functions of impressed voltages, and are nonlinear in nature.

At the system clock rates (up to 2 GHz) and analog bandwidths (up to 10 GHz) for which metal-organic and ceramic multichip modules (MCMs) are being designed [2], [3], it is absolutely necessary to be able to model the propagation of wavefronts through groups of tightly coupled, lossy and dispersive stripline and/or microstrip interconnects, to assure that waveform integrity will be preserved when the actual structures are fabricated and placed into service.

Previous analyses of the problem of modeling the dispersion properties of transmission lines include the spectral domain method [4], and the Fourier transform method [5], among others. Nonlinear terminations have been treated by the harmonic balance technique [6], and the time domain approach [7]. Using Y-parameters, Djordjevic *et al.* [8] introduced augmented networks with negative resistors to match the line impedances. Schutt-Aine and Mittra [9] solved the single line problem by employing S-parameters with a fixed reference impedance on the structure.

Gu *et al.* [10] improved the S-parameter approach, discarded the negative networks and eliminated the fixed reference impedance. These authors discussed general cases of coupled lossy and dispersive transmission lines with nonlinear loads. Nevertheless, the (semi-empirical) dispersion formula (Equation 15 in [10], which has been verified to be accurate to the terahertz range [11]), is valid only for a single microstrip line, and the Newton-Raphson method as employed in [10] may be unstable, particularly when multiple variables are involved. Recently, Mehalic and Mittra [12] expanded the S-parameter approach in conjunction with an iteration-perturbation method [13] so that multiple lines can be treated. However, because resistive line losses were not handled properly in the iteration-perturbation method, the agreement between simulation and measurement was not extremely accurate [1]. In this paper we present a new approach based upon the improved S-parameter method. Improvements to Gu's method [10] are described in this paper, i.e., the use of an unconstrained optimization of the sum of squares of nonlinear functions [14], a more detailed formulation of the scattering matrix for the multiple line case, and a complete derivation of the multiple line networking formulas.

Manuscript received December 5, 1991; revised July 27, 1992. This work was supported under contract N66001-89-C-0104 from the Naval Ocean Systems Center.

The authors are with the Mayo Foundation, Special Purpose Processor Development Group, Rochester, MN 55905.

IEEE Log Number 9205468.

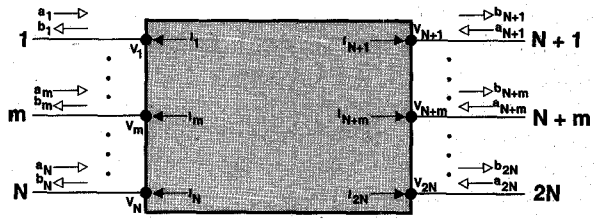

Fig. 1. Schematic diagram of a generalized $2N$-port transmission line system showing current flow conventions.

II. Formulation

2.1 Derivation of Time-Domain Nonlinear Equations

Consider a $2N$-port transmission line system consisting of N coupled lossy and dispersive transmission lines, as illustrated in Fig. 1. The incident wave vector $|\boldsymbol{A}(\omega)\rangle$ and reflected wave vector $|\boldsymbol{B}(\omega)\rangle$ at the terminal ports can be represented as the superposition of port voltage and current vectors $|\boldsymbol{V}(\omega)\rangle$, and $|\boldsymbol{I}(\omega)\rangle$ [15]:

$$|\boldsymbol{A}(\omega)\rangle = \tfrac{1}{2}\{|\boldsymbol{V}(\omega)\rangle - [\boldsymbol{Z}_0(\omega)]|\boldsymbol{I}(\omega)\rangle\} \tag{1}$$

$$|\boldsymbol{B}(\omega)\rangle = \tfrac{1}{2}\{|\boldsymbol{V}(\omega)\rangle + [\boldsymbol{Z}_0(\omega)]|\boldsymbol{I}(\omega)\rangle\} \tag{2}$$

where $[\boldsymbol{Z}_0(\omega)]$ is the characteristic impedance matrix of $2N \times 2N$, which will be defined and formulated later in Section 2.3. Note that the minus and plus signs in the second terms of the above equations may simply be reversed if the directions of current flow are defined oppositely. The incident and reflected voltage waves are related through the scattering matrix $[\boldsymbol{S}(\omega)]$ by:

$$|\boldsymbol{B}(\omega)\rangle = [\boldsymbol{S}(\omega)]|\boldsymbol{A}(\omega)\rangle. \tag{3}$$

Adding (1) and (2), we have:

$$|\boldsymbol{V}(\omega)\rangle = |\boldsymbol{A}(\omega)\rangle + |\boldsymbol{B}(\omega)\rangle. \tag{4}$$

By taking the Fourier transform of (2), (3) and (4), we have the time-domain relations:

$$|\boldsymbol{b}(t)\rangle = \tfrac{1}{2}\left[|\boldsymbol{v}(t)\rangle + \int_0^t d\tau[\boldsymbol{z}_0(t-\tau)]|\boldsymbol{i}(\tau)\rangle\right] \tag{5}$$

$$|\boldsymbol{b}(t)\rangle = \int_0^t d\tau[\boldsymbol{h}(t-\tau)]|\boldsymbol{a}(\tau)\rangle \tag{6}$$

$$|\boldsymbol{v}(t)\rangle = |\boldsymbol{a}(t)\rangle + |\boldsymbol{b}(t)\rangle \tag{7}$$

where $|\boldsymbol{v}(t)\rangle, |\boldsymbol{i}(t)\rangle, |\boldsymbol{a}(t)\rangle, |\boldsymbol{b}(t)\rangle, [\boldsymbol{h}(t)]$ and $[\boldsymbol{z}_0(t)]$ are, respectively, the inverse Fourier transforms of $|\boldsymbol{V}(\omega)\rangle, |\boldsymbol{I}(\omega)\rangle, |\boldsymbol{A}(\omega)\rangle, |\boldsymbol{B}(\omega)\rangle$, $[\boldsymbol{S}(\omega)]$ and $[\boldsymbol{Z}_0(\omega)]$. Note that $[\boldsymbol{h}(t)]$ is the system function matrix of $2N \times 2N$ of the transmission line system, which, by nature, is linear. Therefore, the convolution integral holds. The termination conditions relate the port currents with the voltages as:

$$|\boldsymbol{i}(t)\rangle = |\boldsymbol{f}(|\boldsymbol{v}(t)\rangle)\rangle \tag{8}$$

where $|\boldsymbol{f}(|\boldsymbol{v}(t)\rangle)\rangle$ is, in general, a nonlinear vector function of $|\boldsymbol{v}(t)\rangle$, such as the $I-V$ curves of individual devices. Incorporating the termination conditions (8), we can solve (5), (6) and (7) for four unknowns: $|\boldsymbol{v}(t)\rangle, |\boldsymbol{i}(t)\rangle, |\boldsymbol{a}(t)\rangle$ and $|\boldsymbol{b}(t)\rangle$.

In this paper, we are most interested in the voltage waveforms $|\boldsymbol{v}(t)\rangle$. Note that the nonlinearity is mainly introduced by the nonlinear termination conditions of (8).

2.2 Unconstrained Optimization Techniques

Instead of attempting to solve a set of coupled integral equations, namely, (5)–(8) by the multivariable Newton-Raphson method, which may be numerically unstable, we have utilized optimization techniques. Combining the basic equations (5), (6), (7) and (8), we obtained a set of equations of the port voltages:

$$\int_0^t d\tau[\boldsymbol{h}(t-\tau)]\{|\boldsymbol{v}(\tau)\rangle - |\boldsymbol{q}(|\boldsymbol{v}(\tau)\rangle)\rangle\} = |\boldsymbol{q}(|\boldsymbol{v}(t)\rangle)\rangle \tag{9}$$

and $|\boldsymbol{q}(|\boldsymbol{v}(t)\rangle)\rangle$ represents a vector function of $|\boldsymbol{v}(t)\rangle$ given by

$$|\boldsymbol{q}(|\boldsymbol{v}(t)\rangle)\rangle = \tfrac{1}{2}\left[|\boldsymbol{v}(t)\rangle + \int_0^t d\tau[\boldsymbol{z}_0(t-\tau)]|\boldsymbol{f}(|\boldsymbol{v}(\tau)\rangle)\rangle\right]. \tag{10}$$

To solve the port voltages $|\boldsymbol{v}(t)\rangle$ from (9), we applied the modified Levenberg-Marquardt algorithm with a finite difference Jacobian [14], which minimizes the sum of squares of nonlinear functions. From (9), the functional to be minimized is set up as

$$\begin{aligned}\Psi_{\min}(|\boldsymbol{v}(t)\rangle) &= \left\| \int_0^t d\tau[\boldsymbol{h}(t-\tau)]\{|\boldsymbol{v}(\tau)\rangle - |\boldsymbol{q}(|\boldsymbol{v}(\tau)\rangle)\rangle\} - |\boldsymbol{q}(|\boldsymbol{v}(t)\rangle)\rangle \right\|^2 \\ &= \sum_{m=1}^{2N} \left| \sum_{k=1}^{2N} \int_0^t d\tau\, h_{mk}(t-\tau)\{v_k(\tau) - q_k(|\boldsymbol{v}(\tau)\rangle)\} - q_m(|\boldsymbol{v}(t)\rangle) \right|^2 \end{aligned} \tag{11}$$

where $\|\cdot\|$ denotes the norm of a vector of dimension $2N$, and $|\boldsymbol{q}(|\boldsymbol{v}(t)\rangle)\rangle$ is given by (10). By minimizing the functional of (11), the problem will be completely solved, provided $[\boldsymbol{h}(t)]$ and $[\boldsymbol{z}_0(t)]$ are known. In this paper, the scattering matrix $[\boldsymbol{S}(\omega)]$ and characteristic impedance matrix $[\boldsymbol{Z}_0(\omega)]$ were obtained directly from the volume equivalent principle solutions [1] or from measurements; thus, it is only necessary to take their inverse Fourier transforms. However, in many cases the inductance, capacitance, resistance, and conductance matrices $[\boldsymbol{L}], [\boldsymbol{C}], [\boldsymbol{R}]$ and $[\boldsymbol{G}]$ are given. In the next section we will discuss a more general case of the derivation of the scattering matrix $[\boldsymbol{S}(\omega)]$ and the characteristic impedance matrix $[\boldsymbol{Z}_0(\omega)]$ from the inductance, capacitance, resistance and conductance matrices $[\boldsymbol{L}], [\boldsymbol{C}], [\boldsymbol{R}]$ and $[\boldsymbol{G}]$ as functions of frequency.

2.3 Determination of Frequency Domain Parameters

The voltages and currents on multiconductor transmission lines can be written as follows (the factor $e^{j\omega t}$ is suppressed) [16]:

$$|\boldsymbol{u}(z)\rangle = [\boldsymbol{M}_V]|\boldsymbol{e}(z)\rangle \tag{12}$$

$$|\boldsymbol{i}(z)\rangle = [\boldsymbol{M}_I]|\boldsymbol{j}(z)\rangle \tag{13}$$

where z is the direction of wave propagation along the lines, and the vectors $|\boldsymbol{e}(z)\rangle$ and $|\boldsymbol{j}(z)\rangle$ are the voltages and currents of the eigenmodes, respectively; $[\boldsymbol{M}_V]$ and $[\boldsymbol{M}_I]$ are the voltage eigenvector matrix of $[\boldsymbol{Z}^l][\boldsymbol{Y}^c]$ and current eigenvector matrix of $[\boldsymbol{Y}^c][\boldsymbol{Z}^l]$, respectively. $[\boldsymbol{Z}^l]$ and $[\boldsymbol{Y}^c]$ are given by

$$[\boldsymbol{Z}^l] = [\boldsymbol{L}] - j[\boldsymbol{R}]/\omega \tag{14}$$

$$[\boldsymbol{Y}^c] = [\boldsymbol{C}] - j[\boldsymbol{G}]/\omega. \tag{15}$$

It can be shown that, with the proper choice of eigenvectors:

$$[\boldsymbol{M}_I][\boldsymbol{M}_V]^T = [\boldsymbol{U}] \tag{16}$$

where $[\boldsymbol{U}]$ is the identity matrix. The voltages and currents of the eigenmodes can be expressed by

$$|\boldsymbol{e}(z)\rangle = [\boldsymbol{E}^{(f)}(z)]|\boldsymbol{r}\rangle + [\boldsymbol{E}^{(b)}(z)]|\boldsymbol{p}\rangle \tag{17}$$

$$|\boldsymbol{j}(z)\rangle = [\boldsymbol{E}^{(f)}(z)][\boldsymbol{Z}_d]^{-1}|\boldsymbol{r}\rangle - [\boldsymbol{E}^{(b)}(z)][\boldsymbol{Z}_d]^{-1}|\boldsymbol{p}\rangle \tag{18}$$

where

$$[\boldsymbol{E}^{(f)}(z)] = \operatorname{diag}\{e^{-\gamma_1 z}, e^{-\gamma_2 z}, \cdots, e^{-\gamma_N z}\} \tag{19}$$

$$[\boldsymbol{E}^{(b)}(z)] = \operatorname{diag}\{e^{\gamma_1(z-l)}, e^{\gamma_2(z-l)}, \cdots, e^{\gamma_N(z-l)}\} \tag{20}$$

represent the forward and backward traveling waves, respectively, and

$$[\boldsymbol{Z}_d] = \operatorname{diag}\{Z_1, Z_2, \cdots, Z_N\} \tag{21}$$

where γ_m and $Z_m = \sqrt{Z_m^l / Y_m^c}$ are, respectively, the propagation constant and characteristic impedance of the mth mode. l is the coupling length of the multiconductor transmission lines. $|\boldsymbol{r}\rangle$ and $|\boldsymbol{p}\rangle$ are constants to be found from the boundary conditions. γ_m can be found from eigenvalue λ_m of $[\boldsymbol{Z}^l][\boldsymbol{Y}^c]$ or $[\boldsymbol{Y}^c][\boldsymbol{Z}^l]$ by $\gamma_m = j\omega\sqrt{\lambda_m}$. Z_m^l and Y_m^c are, respectively, the mth diagonal elements of the decoupled (diagonalized) impedance matrix $[\boldsymbol{Z}_d^l]$ and admittance matrix $[\boldsymbol{Y}_d^c]$ which can be calculated from the transformation matrices $[\boldsymbol{M}_V]$ and $[\boldsymbol{M}_I]$ as follows:

$$[\boldsymbol{Z}_d^l] = [\boldsymbol{M}_I]^T[\boldsymbol{Z}^l][\boldsymbol{M}_I] \tag{22}$$

$$[\boldsymbol{Y}_d^c] = [\boldsymbol{M}_V]^T[\boldsymbol{Y}^c][\boldsymbol{M}_V] \tag{23}$$

Let $z = 0$ and l; we can obtain the port voltages and currents

$$\begin{aligned} |\boldsymbol{V}_n\rangle &= |\boldsymbol{u}(0)\rangle = [\boldsymbol{M}_V]|\boldsymbol{r}\rangle + [\boldsymbol{M}_V][\boldsymbol{E}]|\boldsymbol{p}\rangle \\ |\boldsymbol{V}_f\rangle &= |\boldsymbol{u}(l)\rangle = [\boldsymbol{M}_V][\boldsymbol{E}]|\boldsymbol{r}\rangle + [\boldsymbol{M}_V]|\boldsymbol{p}\rangle \\ |\boldsymbol{I}_n\rangle &= -|\boldsymbol{i}(0)\rangle = -[\boldsymbol{M}_I][\boldsymbol{Z}_d]^{-1}|\boldsymbol{r}\rangle + [\boldsymbol{M}_I][\boldsymbol{E}][\boldsymbol{Z}_d]^{-1}|\boldsymbol{p}\rangle \\ |\boldsymbol{I}_f\rangle &= |\boldsymbol{i}(l)\rangle = [\boldsymbol{M}_I][\boldsymbol{E}][\boldsymbol{Z}_d]^{-1}|\boldsymbol{r}\rangle - [\boldsymbol{M}_I][\boldsymbol{Z}_d]^{-1}|\boldsymbol{p}\rangle \end{aligned}$$

where $[\boldsymbol{E}] = [\boldsymbol{E}^{(f)}(l)] = [\boldsymbol{E}^{(b)}(0)]$, and subscripts n and f denote the near and far ends, respectively. Combining the above equations and evaluating the port voltages in terms of the impedance matrix and the port currents, we have:

$$|\boldsymbol{V}\rangle = [\boldsymbol{Z}]|\boldsymbol{I}\rangle \tag{24}$$

where

$$|\boldsymbol{V}\rangle = [|\boldsymbol{V}_n\rangle^T, |\boldsymbol{V}_f\rangle^T]^T$$

$$|\boldsymbol{I}\rangle = [|\boldsymbol{I}_n\rangle^T, |\boldsymbol{I}_f\rangle^T]^T$$

The impedance matrix is given by

$$[Z] = [F_V][F_I]^{-1} \tag{25}$$

where

$$[F_V] = \begin{bmatrix} [M_V] & [M_V][E] \\ [M_V][E] & [M_V] \end{bmatrix}$$

$$[F_I] = \begin{bmatrix} -[M_I][Z_d]^{-1} & [M_I][E][Z_d]^{-1} \\ [M_I][E][Z_d]^{-1} & -[M_I][Z_d - d]^{-1} \end{bmatrix}.$$

The characteristic impedance can be shown to be

$$[Z_0] = \begin{bmatrix} [M_V][Z_d][M_I]^{-1} & [0] \\ [0] & [M_V][Z_d][M_I]^{-1} \end{bmatrix}. \tag{26}$$

Combining (24) and (25), (1) and (2) we obtained

$$|A\rangle = \begin{bmatrix} [M_V]|r\rangle \\ [M_V]|p\rangle \end{bmatrix}. \tag{27}$$

$$|B\rangle = \begin{bmatrix} [M_V][E]|p\rangle \\ [M_V][E]|r\rangle \end{bmatrix}. \tag{28}$$

The above equations imply that $|A\rangle$ and $|B\rangle$ represent, respectively, the incoming and outgoing waves at the terminal ports. Therefore the above choice of the characteristic impedance matrix $[Z_0]$ is reasonable.

Substituting (24) into (1) and (2), evaluating $|B\rangle$ in terms of $|A\rangle$ and comparing with (3), one obtains

$$[S(\omega)] = ([Z(\omega)] + [Z_0(\omega)])([Z(\omega)] - [Z_0(\omega)])^{-1}. \tag{29}$$

Now substituting (25) and (26) into (29), the scattering matrix is found as follows:

$$[S] = \begin{bmatrix} [0] & [M_V][E][M_V]^{-1} \\ [M_V][E][M_V]^{-1} & [0] \end{bmatrix} \tag{30}$$

2.4 Evaluation of Time Domain Parameters

Rewriting the scattering matrix (30) as:

$$[S(\omega)] = \begin{bmatrix} [0] & [S_1(\omega)] \\ [S_1(\omega)] & [0] \end{bmatrix} \tag{31}$$

where

$$[S_1(\omega)] = [S_{mn}(\omega)]_{N\times N} = [M_V][E][M_V]^{-1}. \tag{32}$$

It can be shown that the matrix element $S_{mn}(\omega)$ takes the following form:

$$S_{mn}(\omega) = \sum_{k=1}^{N} S_{mn}^k(\omega) e^{-j\beta_k(\omega)l} \tag{33}$$

where β_k is the imaginary part of γ_k. To deal with the singularity of the inverse Fourier transform of $S_{mn}(\omega)$ due to

$$\lim_{\omega\to\infty} S_{mn}(\omega) \neq 0$$

we separate $S_{mn}(\omega)$ into two parts, as in [10]:

$$S_{mn}(\omega) = S'_{mn}(\omega) + S_{mn}(\infty) \tag{34}$$

where

$$S'_{mn}(\omega) = \sum_{k=1}^{N} S_{mn}^k(\infty) e^{-j\beta_k(\infty)l} \cdot \left[\frac{S_{mn}^k(\omega)}{S_{mn}^k(\infty)} e^{-j[\beta_k(\omega)-\beta_k(\infty)]l} - 1\right]$$

$$S_{mn}(\infty) = \sum_{k=1}^{N} S_{mn}^k(\infty) e^{-j\beta'_k(\infty)\omega l}$$

Obviously, $S_{mn}(\infty)$ can be inverse transformed analytically to obtain a series of impulse functions which correspond to the time delays of the modes, and $S'_{mn}(\omega)$ is well-behaved and integrable ($S'_{mn}(\omega)$ approaches 0 as ω approaches infinity). The latter expression represents the contribution of $[S(\omega)]$ due to dispersion. The inverse Fourier transform of $S_{mn}(\omega)$ is:

$$h_{mn}(t) = h'_{mn}(t) + \sum_{k=1}^{N} \delta(t - \tau_k) S_{mn}^k(\infty) \tag{35}$$

where $h'_{mn}(t)$ is the inverse Fourier transform of $S'_{mn}(\omega)$, and $\tau_k = \beta_k(\infty)l/\omega = \beta'_k(\infty)l$ is the time delay of the kth mode.

We rewrite the characteristic impedance matrix as:

$$[Z_0(\omega)] = \begin{bmatrix} [Z_{01}(\omega)] & [0] \\ [0] & [Z_{01}(\omega)] \end{bmatrix} \tag{36}$$

where

$$[Z_{01}(\omega)] = [Z_{0mn}(\omega)]_{N\times N} = [M_V][Z_d][M_I]^{-1} \tag{37}$$

The calculation of $z_{0mn}(t)$ is similar to that of $h_{mn}(t)$. Separating $Z_{0mn}(\omega)$ into two parts,

$$Z_{0mn}(\omega) = Z'_{0mn}(\omega) + Z_{0mn}(\infty) \tag{38}$$

where

$$Z'_{0mn}(\omega) = Z_{0mn}(\infty)\left[\frac{Z_{0mn}(\omega)}{Z_{0mn}(\infty)} - 1\right]$$

The inverse Fourier transform of $Z_{0mn}(\omega)$ becomes:

$$z_{0mn}(t) = z'_{0mn}(t) + \delta(t) Z_{0mn}(\infty) \tag{39}$$

where $z'_{0mn}(t)$ is the inverse Fourier transform of $Z'_{0mn}(\omega)$.

III. Numerical Examples

To demonstrate the effectiveness and generality of the new method described in this paper, five examples will be presented. In the first four, we will compare our results with data from the literature; agreement of the results of the new method with the data from four papers employing four different algorithms are all quite impressive. The last example deals with a very general case of three coupled lossy and dispersive microstrips with nonlinear loads. Laboratory experiments are being established to yield measured data to compare with the calculated results.

Example 1. A single dispersive microstrip line terminated with a nonlinear load was discussed by Gu *et al.* as Example 1 in [10]. We repeated the simulation with the same data (geometry, source and termination conditions, etc.); Fig. 2 compares our results with Fig. 6 of [10]. Agreement of results as presented in these two figures is good, except that the secondary reflection at the far end of the line is larger in our results, which appears to be more reasonable because the line is assumed lossless and the source impedance is not perfectly matched with the line.

Example 2. A square pulse propagating along a dispersive microstrip line with a matched load was studied by Veghte and Balanis [5]. Using the same data given in their Fig. 4, our method generated the same results. The comparison of our results with those of Veghte is shown in Fig. 3. The agreement between the two sets of results is excellent.

Example 3. To compare our results with laboratory measurements, we employed an example of a lossless stripline terminated with

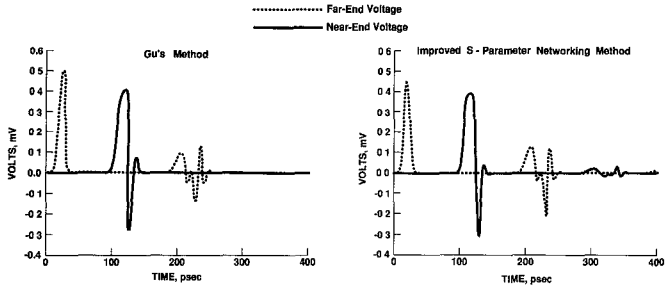

Fig. 2. Comparison of simulation results of single dispersive microstrip transmission line using Gu's method and the improved S-parameter networking method. Left panel: Gu's results. Right panel: results obtained with this method.

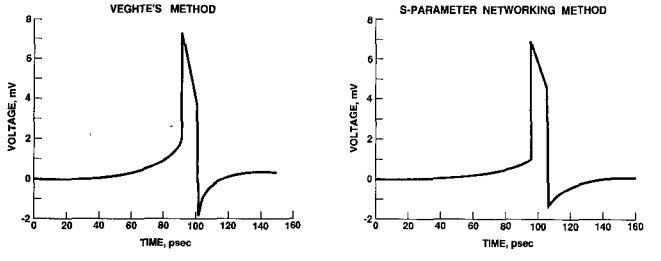

Fig. 3. Comparison of simulation results of lossy dispersive microstrip transmission line using Veghte's method and the improved S-parameter networking method. Left panel: Veghte's results. Right panel: results obtained with this method.

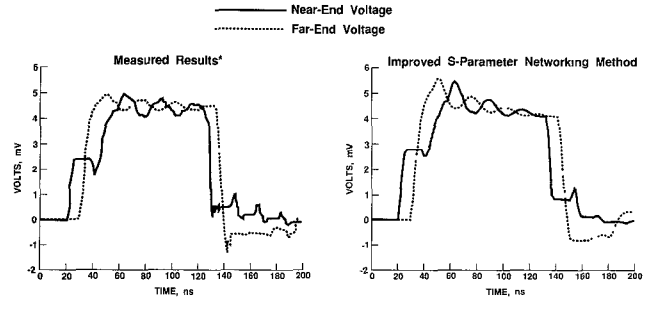

Fig. 4. Comparison of measured results from single microstrip transmission line from Schutt-Aine and Mittra, and simulations of the same line using the improved S-parameter networking method. Left panel: measured line responses. Right panel: simulated results obtained with this method.

advanced Schottky TTL inverters, as depicted in Fig. 7 of Schutt-Aine and Mittra [9], in which the transmission line is lossless and dispersionless, and the device has been simplified but its nonlineality retained. We used all the information presented in [9], including electrical and geometric data, and the nonlinear I-V curves for a simplified model of a TTL gate (i.e., a nonlinear back biased diode in parallel with a capacitor) provided in [9], and duplicated the waveforms and compared them with the photographs in Fig. 4. Overall, good agreement between the two sets of results is demonstrated.

Example 4. In this example we compared our results with the numerical example of Djordjevic *et al.* in [8], where the two far-end loads are nonlinear, and the two transmission lines are lossy and coupled. The frequency dependent behavior was simplified by considering only skin effect loss, with the resistance proportional to the square root of the operating frequency. This simplification may not be accurate especially for transmission lines whose cross sectional dimensions are on the same order of the skin depth, as a result, dispersion was not fully addressed. Using Djordjevic's line

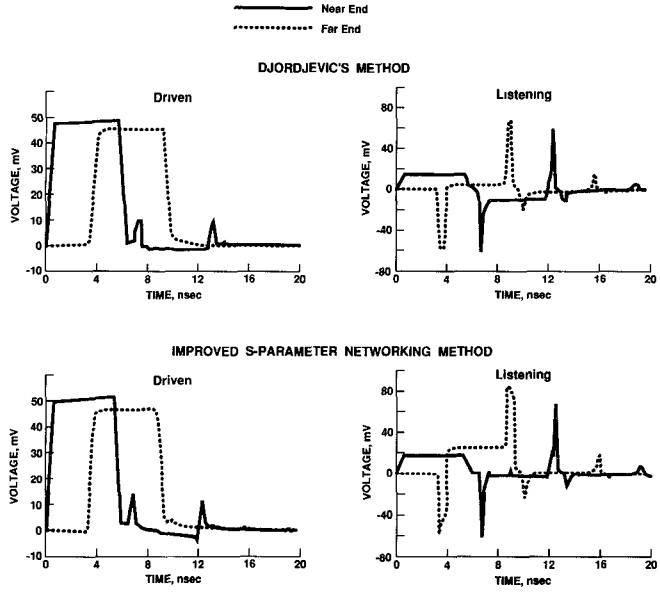

Fig. 5. Comparison of simulation results of coupled lossy, dispersive microstrip transmission lines using Djordjevic's method and the improved S-parameter networking method. Upper panels: Djordjevic's results. Lower panels: results obtained with this method.

parameters, our results agreed very well with Djordjevic *et al.*, as illustrated in Fig. 5.

Example 5. In all the previous examples, the combined effect of three factors, namely, load nonlinearity, line coupling and dispersion has never been investigated. In fact, among the three factors, only one or two have been studied at a time. Therefore, we present here a complete analysis of a total combination of all three factors. First, we needed a set of data that reveals frequency dependent characteristics (dispersion, frequency dependent losses and so on) of a set of coupled transmission lines. This was accomplished by the volume equivalent principle approach in a separate paper [1], where the S-parameters and the characteristic impedance matrix of the three coupled microstrip lines depicted schematically in the upper two panels of Fig. 6 were obtained.

It should be noted that the structure which was simulated for this example is a section of an actual passive test coupon designed in the Mayo laboratory, fabricated by Honeywell Corporation using their Thin Film Multilayer (TFML) copper-polyimide multichip module process, and presently undergoing extensive testing at Mayo [2]. The S-parameter and characteristic impedance matrix data derived from the Honeywell test coupon simulations, taking coupling, losses and dispersion into account, were then utilized in our nonlinear loads program. A complete picture of waveform distortion and crosstalk as a result of the combined effect of load nonlinearity, line loss, dispersion and coupling, are illustrated in the three lower panels of Fig. 6. No comparison from the literature is available at present; however, measured data from our own laboratories will be available in the near future. Finally, Fig. 7 shows the simulated S-parameter data from the first step of this process based upon the structural parameters of the Honeywell coupon, and S-parameters measured with the HP 8510B network analyzer.

IV. Conclusions

In this paper, a technique based upon an improved S-parameter and unconstrained optimization method has been described for the analysis of the wavefront propagation characteristics of coupled lossy and dispersive transmission lines terminated with nonlinear loads. A

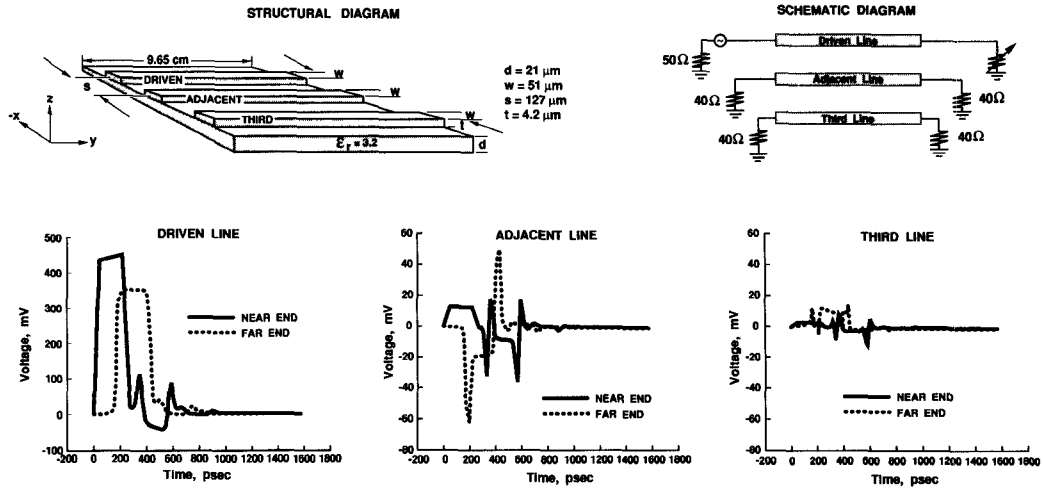

Fig. 6. Simulation results of lossy transmission lines with nonlinear loads calculated with the improved S-parameter networking method. Upper left: structural diagram of the simulated three line structure. Upper right: schematic diagram of the simulated three line structure. Lower left: waveforms on driven line. Lower middle: waveforms on adjacent line. Lower right: waveforms on third line.

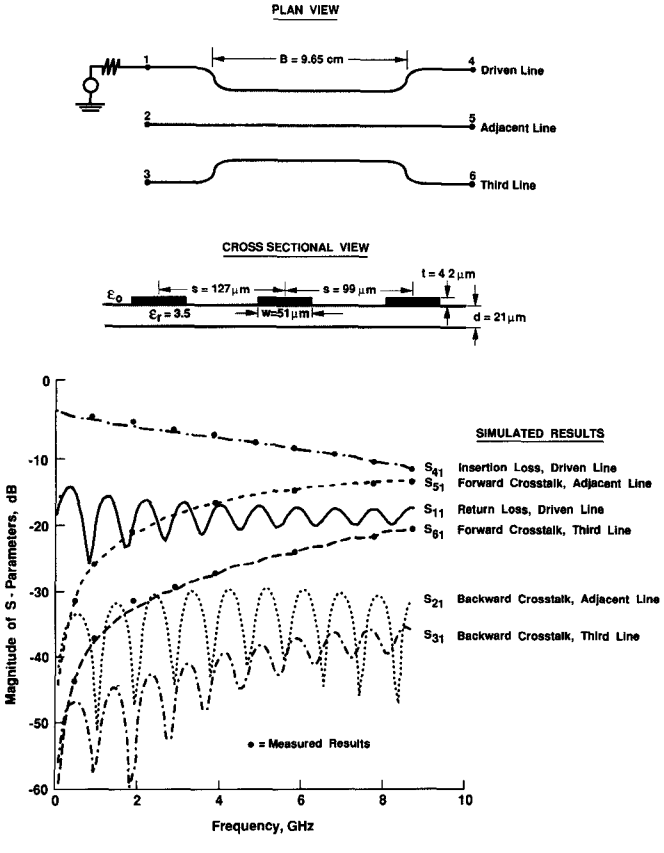

Fig. 7. Simulated and measured scattering parameters and structural features for copper-polyimide Thin Film Multilayer (TFML) multichip module; simulations based on results of Wang *et al.* TFML coupon fabricated by Honeywell SSEC; measurements with HP 8510B network analyzer and Cascade microwave probes.

modal analysis of multiple transmission lines is also discussed. As a more general and effective method, this approach generates the results of many previous methods as special cases.

REFERENCES

[1] G. Pan, J. Tan, and B. Gilbert, "Notes on skin effect and dispersion of heavily lossy transmission lines with extremely small cross sections," in Preparation.

[2] B. K. Gilbert, W. I. McNeff, P. J. Zabinski, W. P. Kornrumpf, S. F. Tead, R. L. Maki, K. E. Carolson, and J. E. Gerber, "Development of deposited multichip modules with unique features for application in GaAs signal processors operating above 1 GHz clock rates," *Proc. Int. Electronic Packaging Society,* Sept. 1991.

[3] B. K. Gilbert and G. W. Pan, "Packaging of GaAs signal processors on multichip modules," *IEEE Trans. Comp. Hybrids, Manuf. Technol*, vol. 15, no. 1, pp. 15–28, Feb. 1992.

[4] T. Itoh and R. Mittra, "Spectral-domain approach for calculating the dispersion characteristics of microstrip lines," *IEEE Trans. Microwave Theory Tech.*, vol. MTT-21, pp. 496–499, July 1973.

[5] R. L. Veghte and C. A. Balanis, "Dispersion of transient signals in microstrip transmission lines," *IEEE Trans. Microwave Theory Tech.*, vol. MTT-34, pp. 1427–1436, Dec. 1986.

[6] K. S. Kundert, G. B. Sorkin, and A. Sangiovanni-Vincentelli, "Applying harmonic balance to almost-periodic circuits," *IEEE Trans Microwave Theory Tech.*, vol. 36, pp. 366–378, Feb. 1988.

[7] T. K. Liu and F. M. Tesche, "Analysis of antennas and scatterers with nonlinear loads," *IEEE Transactions Antennas Propagat.*, vol. AP-24, pp. 131–139, 1976.

[8] A. R. Djordjevic, T. K. Sarkar, and R. F. Harrington, "Analysis of lossy transmission lines with arbitrary nonlinear terminal networks," *IEEE Trans. Microwave Theory Tech*, vol. MTT-34, pp. 660–666, June 1986.

[9] J. E. Schutt-Aine and R. Mittra, "Scattering parameter transient analysis of transmission lines loaded with nonlinear terminations," *IEEE Trans. Microwave Theory Tech.*, vol. 36, pp. 529–536, Mar. 1988.

[10] Q. Gu, Y. E. Yang, and J. A. Kong. "Transient analysis of frequency-dependent transmission line systems terminated with nonlinear loads," *J. Electro. Waves Applic.*, vol. 3, pp. 183–197, Mar. 1989.

[11] M. Y. Frankel, S. Gupta, J. A. Valdmanis, and G. A. Mourou, "Terahertz attenuation and dispersion characteristics of coplanar transmission lines," *IEEE Trans. Microwave Theory Tech.*, vol. 39, pp. 910–916, June 1991.

[12] M. Mehalic and R. Mittra, "Investigation of tapered multiple microstrip lines for VLSI circuits," *IEEE Trans. Microwave Theory Tech.*, vol. 38, pp. 1559–1566, Nov. 1990.

[13] R. E. Collin, *Field Theory of Guided Waves,* 2nd ed., The Institute of Electrical and Electronics Engineers, Inc., New York, 1991.

[14] J. E. Dennis and R. B. Schnabel, *Numerical Methods for Unconstrained Optimization and Nonlinear Equations.* Englewood Cliffs, NJ: Prentice-Hall, 1983.

[15] S. Y. Liao, *Microwave Devices and Circuits.* Englewood Cliffs, NJ: Prentice-Hall, 07632, 1985, pp. 158–160.

[16] G. W. Pan, K. S. Olson, and B. K. Gilbert, "Improved algorithmic methods for the prediction of wavefront propagation behavior in multiconductor transmission lines for high frequency digital signal processors," *IEEE Trans. Computer-Aided Design,* vol. 8, pp. 608–621, June 1989.